International Journal of Oil, Gas and Coal Engineering
2014; 2(3): 36-54
Published online July 20, 2014 (http://www.sciencepublishinggroup.com/j/ogce)
doi: 10.11648/j.ogce.20140203.12

Investigation of fluid properties and their effect on seismic response: A case study of Fenchuganj gas field, Surma Basin, Bangladesh

S. M. Ariful Islam[1], Md Shofiqul Islam[1, *], Mohammad Moinul Hossain[2]

[1]Department of Petroleum and Mining Engineering, Shahjalal University of Science and Technology, Sylhet 3114 Bangladesh
[2]Geophysical division, Bangladesh Petroleum Exploration and Production Company (BAPEX), Dhaka, Bangladesh

Email address:
Sho_fiq@yahoo.com (Md S. Islam)

To cite this article:
S. M. Ariful Islam, Md Shofiqul Islam, Mohammad Moinul Hossain. Investigation of Fluid Properties and their Effect on Seismic Response: A Case Study of Fenchuganj Gas Field, Surma Basin, Bangladesh. *International Journal of Oil, Gas and Coal Engineering*. Vol. 2, No. 3, 2014, pp. 36-54. doi: 10.11648/j.ogce.20140203.12

Abstract: The Fenchuganj Gas Field is one of the water-drive gas fields in the Surma Basin, Bangladesh. Due to gas production water saturation is increasing day by day. However, fluid properties of the reservoir at the present state in the gas depleted condition should be addressed with proper prediction. In this paper, we represent some modeling results which evidences that the pore fluids have a significant effect on the acoustic impedance and the Poisson's ratio of the reservoir rock which is directly correlated with seismic amplitudes at constant pressure with Batzle-Wang model and Gassman-Boit models. Moreover, these models with varying pressure and water saturation conditions show the reasonable predicted fluid modulus against pressure. The reservoir modeling from irreducible water saturation conditions (90% gas saturation) to residual gas conditions (10% gas saturation) provides a pathway to calculate values at reservoir conditions from logging conditions. Fluid bulk density increases when water saturation increases with constant pressure and stay around constant when water saturation increases with pressure fall. But overall it increases through the production path that we assumed. Amplitude versus Offset (AVO) analysis also consistent with other studies models which show that seismic reflection of p-wave changes due to change of pressure and water saturation of the reservoir rock layers. The AVO response decreases with increases of water saturation of the gas zones. The evaluation of fluid properties enables seismic data to be used more powerfully. This study is also showing that both gas zones of the Fenchuganj are under gas sand category 3. We suggest that the modeling of fluid property in determining the usefulness of time lapse seismic, predicting AVO and amplitude response, and making production and reservoir engineering decisions and forecasting in the study field.

Keywords: Fluid, Reservoir, Gas Sand, Saturation, and AVO

1. Introduction

Reservoir characterization is a model of a reservoir that incorporates all the characteristics of the reservoir that are relevant to its ability to store hydrocarbons and also to produce them. Reservoir characterization models are used to suggest the behavior of the fluids within the reservoir under different sets of situation and to find the best possible production techniques that will maximize the production.

However, the seismic data is commonly used for interpretation and evaluation of structural or stratigraphic features in the subsurface. The physical properties of pore fluids have an effect on the seismic response of a porous rock containing those fluids. It is necessary to have an understanding of the changes in p-wave (compressional) velocity, s-wave (shear) velocity, and density as fluid or rock properties change to recognize or predict the effect of changes in seismic amplitudes and travel times.

Different methods are used to determine the fluid properties from well log and seismic data (e.g., [1,2,3,4,5,6,7,8,9,10]). However, we have used Batzle and Wang [8] model, Gassmann [2] -Biot [3] model and AVO (Zoeppritz equation) model for this work. The Batzle and Wang [8] model determines fluid properties, whereas, the Gassmann-Biot model predicts the saturated rock properties in reservoir rock matrix and gives a forecast of future effects of saturated rock properties on seismic response. Moreover, the AVO (amplitude variation with

offset) model predicts the seismic response from the layered rock properties [11].

In geophysics and reflection seismology, amplitude versus offset (AVO) or amplitude variation with offset is the general term for referring to the dependency of the seismic attribute, amplitude, with the distance between the source and receiver (the offset). AVO analysis is a technique that geophysicists can accomplish on seismic data to determine a rock's fluid content, porosity, density or seismic velocity, shear wave information, fluid indicators (hydrocarbon indications [17]).

The P-wave and S-wave velocity, bulk density, acoustic impedance, Poisson's ratio (PR), and bulk modulus are determined from Batzle and Wang [8] without considering the rock matrix and from Gassmann-Biot models as a function of the saturating rock fluids. Fenchuganj Gas Field is one of major producing gas fields in the Surma basin (a petroliferous basin in Bangladesh) with estimated reserves of 553 Bcf [12]. However, till now there is no work yet to be done on Fenchuganj Gas Field using seismic response to predict fluid properties. So there is a big appeal to forecast reservoir properties using seismic/well log data. Our aim is i) to predict the velocity, density and modulus of fluid samples for both constant/varying saturation with constant/varying pressure using Batzle and Wang model and Gassmann-Biot model, and ii) to predict seismic response from the layered rock properties using AVO (Zoeppritz equation) for New Gas Zone III and New Gas Zone II of Fenchuganj Gas Field.

2. Geological Setting and Stratigraphy of the Study Area

The study area is under Fenchuganj structure which situated in the transition zone between the central Surma Basin and the folded belt in the east and is closest to the eastern margin of the central Surma Basin. It is surrounded by different gas fields with Miocene reservoirs, such as Kailas Tilain the north, Beani Bazar in the east and Rashidpur in the south. It is separated in the north from Kailas Tila and in the south from the Batchia anticline by a clear saddle. From available geological and geophysical data of the Surma Basin, it appears that the Fenchuganj structure is the third highest structure after Chattak and Atgram in the Surma Basin. Fenchuganj is a comparatively young structure and contemporaneous with Atgram, Chattak and DupiTila structures and older than Kailashtila, Beani Bazar, Sylhet etc. Available data suggest that the structural growth of this structure began after deposition of the Upper Marine Shale (uppermost Miocene) and at the beginning of the Dupi Tila a small dip closure anticline had already taken shape. It is believed that the main anticlinal shaping and uplifting took place during and after DupiTila time, which climaxed in the erosion of the base of the Dupi Tila within the crestal part. Finally, this resulted in the faulting of the structure, creating a reverse fault, and making the eastern flank of the anticline steeper. It is most likely that the structural growth is still continuing.

Table 1. *Lithostratigraphic succession of Fenchuganj Gas Field (after [12,13]).*

Age	Formation	Depth (m)	Thickness (m)	Lithology
Recent	Alluvium	0-30	30	Unconsolidated sand, silt and clay
Late Pliocene	DupiTila	30-298	268	Mostly sandstone and minor clay. Sandstone: Brown to light brown, coarse sand
Middle Pliocene	Tipam	298-1150	852	Mostly sandstone and minor clay. Sandstones are light to off white, medium, ferruginous, poorly consolidated, and composed of mainly quartz with few mica & dark color minerals
Miocene	Upper Bokabil	1150-1466	316	Grey to bluish grey shale, soft to moderately hard and compact, and also laminated.
	Middle Bokabil	1466-1766	300	Sandstone and shale alteration
	Lower Bokabil	1766-2236	470	Mostly shale with minor sandstone
Early Miocene	Upper Bhuban	2236- down to 4977	914-2741 (Vary)	Alternation of sandstone and shale, with minor calcareous siltstone

Geology of the Fenchuganj gas field is similar to that of other fields situated in Surma basin. The reservoirs have been found in the Miocene sediments, mainly composed of alternating gray to dark gray clay, very fine to medium grained sandstones. The problem of identifying source rocks is compounded by the fact that the known hydrocarbon accumulated in traps formed in Plio-Pleistocene time [13]. The gas- condensate and oil must have migrated relatively long distances into the traps because the shale's inter bedded with or adjacent to the reservoirs are both organically lean and immature for hydrocarbon generation. It seems most likely that the source rocks of the gas-condensate are the Lower Miocene to Upper Oligocene shale in the basin center and in the synclinal troughs between the fold trends [12]. The source rocks are terrestrial in origin [14].

In Bangladesh, a stratigraphic subdivision of the rock sequence (Table 1) follows the broad tectonic divisions of the country. Between the two stratigraphic subdivisions 1) Stable platform and 2) Bengal foredeep; the second group is categorized by a thick deposit of mostly continental gas bearing clastic sediments of Neogene age characterize the basinal or geosynclinal facies of Bangladesh [14]. Fenchuganj structure belongs to Bengal

foredeep (Geosynclinal) Basin. The stratigraphic succession of Fenchuganj Gas field is based on geological data, seismic data and well data. Stratigraphic succession with a brief lithological description of Fenchuganj gas field is given in Table 1. The sediments of Fenchuganj structure are consisting of alteration shale and sandstone with varying proportions of Oligocene to recent age [13].

3. Methodology

Fig. 1 is a generalized flow chart for seismic reservoir modeling showing the relationship of fluid properties to seismic response, where AVO modeling is the end result of this work. Firstly, we obtained input values from well test data. Then we determined fluid properties and saturating rock properties respectively from Batzle and Wang [8], and Gassmann–Biot [2,3] model for varying saturation with constant pressure condition. Again, we did the same for varying saturation and pressure condition. Moreover, the calculation of AVO from Zoeppritz equation was also performed.

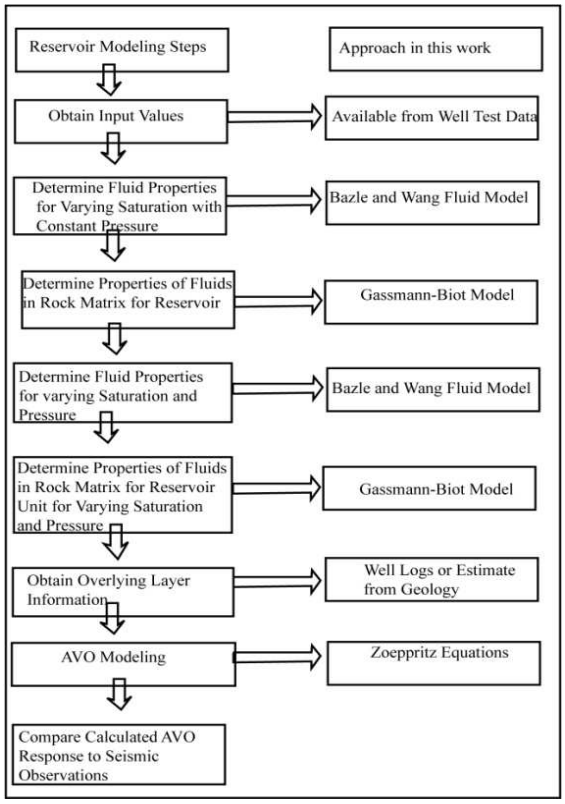

Fig. 1. *A generalized flow chart for seismic reservoir modeling showing the relationship of fluid properties to seismic response.*

3.1. Batzle and Wang Fluid Property Model

In 1992, M. Batzle and Z. Wang [8] introduced a model combing the thermodynamic relationships and empirical trends to predict the effects of pressure, temperature, and composition on the seismic properties of fluids. These authors examined the properties of the three primary types of pore fluids (gases, oils, and brines) in most of the reservoir. The fluid properties predicted include density and bulk modulus (and therefore velocity) as the functions of fluid temperature and pressure, when the pore fluid composition is known or estimated.

This method needs some basic input variables such as reservoir temperature (T, in °C), reservoir pressure (P, in MPa), gas specific gravity (G), Gas-Oil Ratio (GOR) (Rg), degree API gravity of oil (°API), salinity (S, in ppm), gas saturation percentage (Sg), oil saturation percentage (So) and brine saturation percentage (Sb), and some constant values such as density of air (ρair) and gas constant (R) for calculations, which are determined from pressure-volume-temperature (PVT) testing of an oil or fluid sample or estimated from analog information, if available for a nearby area.

3.2. Gassmann-Biot Rock and Fluid Model

P. Gassmann [2] and M. A. Biot [3] developed fundamental and relatively simple relationships to predict the velocities of porous media using global or bulk rock and fluid properties without referring to any specific pore geometry [15]. Gassmann's equations are equivalent to Biot's at low (seismic) frequencies. The low-frequency Gassmann-Biot theory predicts the resulting increase in effective bulk modulus of the saturated rock when the pore pressure changes as a seismic wave passes through the rock [18]. The equations of these models assume a homogeneous mineral modulus and isotropic pore space and the effects of pressure on the dry frame modulus which were not addressed here.

There some input variables such as porosity (ϕ), solid material bulk modulus (KS), solid material density (ρs), water bulk modulus (kW), water density (ρw), hydrocarbon bulk modulus (Khyd), hydrocarbon density (ρhyd), water saturation (SW), logged P-wave velocity (Vpi), logged S-wave velocity (Vsi), logged bulk density (ρbi) and fluid bulk modulus (Kfi) at logged conditions are necessary for the Gassmann-Biot model calculations. The solid material grain bulk modulus and density are determined from the mineralogy of the reservoir matrix. The water/brine and hydrocarbon bulk modulus and density values are computed at reservoir temperature and pressure conditions in the spreadsheet created for the Batzle and Wang [8] model described in section 3.1. The P- and S- wave velocities, and bulk density (Vpi, Vsi, ρbi) values are obtained from well logs and used to calculate the saturated bulk modulus (kBs) and the dry frame shear modulus (G). Gassmann's relations are used to calculate the dry frame bulk modulus (Kdf) using the saturated bulk modulus (kBs, determined from well log or laboratory tests).

The bulk density (ρb) is calculated using a volume weighted average density for the reservoir. The fluid bulk modulus (Kf) is computed using the Reuss (isostress) average is calculated using the water and hydrocarbon saturations. The saturated bulk modulus (KB) is computed at any desired saturation conditions using the dry frame bulk modulus, solid material bulk modulus, fluid modulus,

and porosity. The compressional and shear velocities (VP, Vs) are calculated using a velocity form of Gassmann's relation suggested by Murphy, et al. [16]. All the basic equations (1-10) for calculation of Gassmann-Biot model are given below.

Saturated Bulk Modulus, kBs, in GPA:

$$K_{bs} = \left(\rho_{bi}\left(V_{pi}^2 - \left(\frac{4}{3}V_{si}^2\right)\right)\right)10^{-6} \quad (1)$$

Dry Frame Bulk Modulus, Kdf, in GPa:

$$K_{df} = K_{bs}\left(\frac{(\Phi-1)+\frac{K_s}{K_{bs}}-\Phi\frac{K_s}{K_{fi}}}{(\Phi+1)+\frac{K_{bs}}{K_s}-\Phi\frac{K_{fi}}{K_s}}\right) \quad (2)$$

Dry Frame Shear Modulus-Rigidity, G, in GPa:

$$G = (V_{si}^2\rho_{bi})10^{-6} \quad (3)$$

Bulk Density, ρb, in g/cm3:

$$\rho_b = (1-\Phi)\rho_s + \Phi S_w\rho_w + (1-S_w)\rho_{hyd}\Phi \quad (4)$$

Fluid Bulk Modulus, Kf, in GPa:

$$K_f = \frac{1}{\left(\frac{(1-S_W)}{K_{hyd}}+\frac{S_W}{K_W}\right)} \quad (5)$$

Saturated Bulk Modulus, Kb, in GPa:

$$K_b = \frac{K_{df}+\left(K_s-K_{df}\right)^2}{K_s(1-\Phi)-K_{df}+\Phi\left(\frac{K_s}{K_f}\right)} \quad (6)$$

P-Wave Velocity, Vp, in m/s:

$$V_p = \left[\frac{(K_b+\frac{4}{3}G)}{\rho_b}\right]^{0.5} 10^3 \quad (7)$$

S-Wave Velocity, Vs, in m/s:

$$V_s = \sqrt{\frac{G}{\rho_b}}10^3 \quad (8)$$

Poisson's Ratio, σ:

$$\sigma = 0.5\frac{\left(\frac{V_p}{V_s}\right)^2-2}{\left(\frac{V_p}{V_s}\right)^2-1} \quad (9)$$

Acoustic impedance, AI:

$$AI = V_p\rho_b \quad (10)$$

Using these equations with the necessary input variables allows calculation of the overall reservoir properties taking into account the porosity, rock properties, and fluid properties.

Now that a means for calculating the properties of the reservoir unit have been defined, Zoeppritz equations can be applied to model the AVO response, if the overlying layer information is known.

3.3. Amplitude Versus Offset (AVO) Model: Theory

In geophysics and reflection seismology, amplitude versus offset (AVO) or amplitude variation with offset is the general term for referring to the dependency of the seismic attribute, amplitude, with the distance between the source and receiver (the offset). AVO analysis is a technique that geophysicists can execute on seismic data to determine a rock's fluid content, porosity, density or seismic velocity, shear wave information, fluid indicators [17].

The phenomenon is based on the relationship between the reflection coefficient and the angle of incidence and has been understood since the early 20th century when Karl Zoeppritz wrote down the Zoeppritz equations. Due to its physical origin, AVO can also be known as amplitude versus angle (AVA), but AVO is the more commonly used term because the offset is what a geophysicist can vary in order to change the angle of incidence. AVO computes the seismic response of an interface between two beds from the contrast in elastic properties between the overlying and underlying formations. A normal incident, or zero offset, reflection (Ro) is readily found from the contrast in acoustic impedance.

$$R_o = \frac{\rho_2V_2 - \rho_1V_1}{\rho_2V_2 + \rho_1V_1}$$

Where, Ro = Reflection Coefficient, ρ1 = Density of medium 1, ρ2 = Density of medium 2, V1 = Velocity in medium 1 and V2 = Velocity in medium 2. The change in amplitude of the reflection coefficient with offset is a function of the contrast in elastic properties across the interface.

Rutherford and Williams [6] classify AVO responses into three classes (Fig. 2 (a)) such as 1) A Class I AVO response has a large positive reflection at zero offset and becomes smaller with increasing offset, 2) A Class II AVO response has a small positive reflection at zero offset and becomes very small or even negative with increasing offset, and 3) A Class III AVO response has a negative reflection at zero offset and increasingly large negative reflections at increasing offsets. This is the classical AVO behavior. For example, a sand-shale interface often displays a negative reflection response that is increasingly large with offset.

Castagna and Swan [10] also classified AVO response into four classes (Fig. 2 (b)). First three classes are same as Rutherford and Williams [6], just class IV AVO response has a negative reflection at zero offset and decreasingly negative reflections at increasing offsets.

Zoeppritz equations express the energy partitioning at a boundary when a plane wave impinges on an acoustic impedance contrast [9]. At a boundary where the incident angle is zero (normal incidence) there is no mode conversion. Zoeppritz equations can be used to determine the amplitude of reflected and refracted waves at this boundary for an incident P-wave. The original equations are valid for any incident waves, but only the P-wave is

presented here and used in this study. The reflection and transmission coefficients depend on the angle of incidence and the material properties of the two layers [18]. The angles of incident, reflected, and transmitted rays at a boundary are related by Snell's law [19]. The variation of reflection and transmission coefficients with incident angle and corresponding increasing offset is referred to as offset-dependant-reflectivity and is the fundamental basis for AVO [19].

Zoeppritz [1] equations provide a complete solution for amplitudes of transmitted and reflected P- and S- waves for both incident P- and S- waves. The equations are very complex and subject to troublesome significant, convention, or typographic errors [20] and Aki and Richards [21], Shuey [22], and Hilterman [23] developed simplifications and approximations for Zoeppritz equations. Aki and Richards [21] derived a simplified form of Zoeppritz equations by assuming a small contrasts in properties between layers, where the results are expressed in terms of p-wave velocity, s-wave velocity, and density contrasts across the interface. Shuey [22] presented another approximation to Zoeppritz equations were the AVO gradient is expressed in terms of Poisson's ratio (σ). Due to the complexity of Zoeppritz equations, approximations are extremely useful for application. The most commonly used forms, due to Shuey [22], is given below (valid for incidence angles less than 30 degrees):

Zoeppritz Equation: $R(\theta) = A + B \sin^2(\theta)$

$$A = \frac{1}{2}\left(\frac{\Delta V_p}{V_p} + \frac{\Delta \rho}{\rho}\right)$$

$$B = A_o A + \frac{\Delta \sigma}{(1-\sigma)^2}$$

Where, R (θ) = reflection coefficient (function of θ), θ= angle of incidence, A = zero-offset reflection coefficient (AVO intercept) and B = slope of the amplitude (AVO Gradient).

In this work a simplified AVO calculator is used for AVO analysis that is made by T. B. Berge.

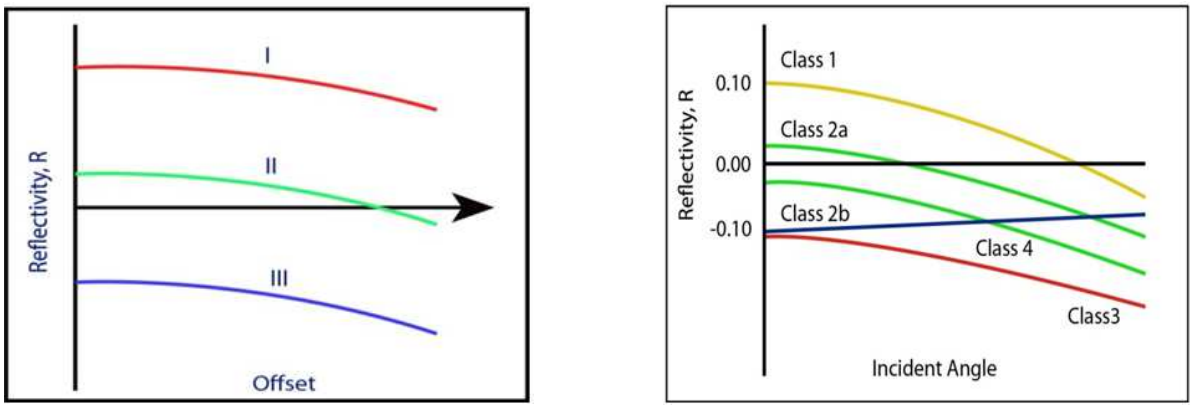

a. b.

Fig. 2. *Plot showing the different classes of AVO response a) reflection amplitude versus offset [6], and b) amplitude versus incident angle [10].*

4. Result and Discussion

There are four gas bearing zones (New Gas Zone III, New Gas Zone II, Upper Gas Zone, New Gas Zone I) were identified in the Fenchuganj gas field. Analysis of two gas zones are presented in this paper while analysis of others two gas zones will publish elsewhere. New Gas Zone III was found at a depth of 1656-1680m, with pressure 16.3888 MPa (2377 psi), temperature 46.67 °C (116 °F), porosity 27.3%, gas saturation 54%, water saturation 46% and salinity 8500 ppm. The New Gas Zone II with depth 1992-2017m, pressure 19.7328 MPa (2862 psi), temperature 51.11 °C (124 °F), porosity 14.5%, gas saturation 36%, water saturation 64% and salinity 9500 ppm. For both gas zones, density of air is 0.00122 g/cc, the API gravity of condensate is 31.86°, gas-condensate ratio is 142260, gas constant (R) is 8.3145, and specific gravity of gas is 0.5624. These are the initial conditions of New Gas Zone III and II (also listed in table 2). Fluid properties for both zones were analyzed using the aforementioned methods in section 3. Our main aim was to investigate and forecast the behavior of reservoir fluid properties during production are discussed through section 4.1 to 4.2.

4.1. Fluid models for Varying Saturation Under Constant Pressure

4.1.1. Batzle and Wang Model

Using initial conditions, i.e. parameters for Batzle and Wang model for varying saturation with constant pressure, we have calculated density (ρ), acoustic velocity (VP) and modulus (k) of gas, brine and mixture phase (Table 3).

The calculated result shows that the density (ρ), acoustic velocity (Vp) and bulk modulus (k) are 0.1151 g/cm3, 526.31 m/s, and 31.88 MPa for New Gas Zone III, whereas New gas Zone II shows these values are 0.1346 g/cm3,

Table 2. *Input Values for Batzle and Wang Model.*

Gas Zones	Measured Depth, m	Pressure, MPa	Temperature, °C	Porosity, Φ	Gas Saturation, Sg	Water Saturation, Sw	Salinity, ppm
New Gas Zone III	1656-1680	16.3888	46.67	0.273	0.54	0.46	8500
New Gas Zone II	1992-2017	19.7328	51.11	0.145	0.36	0.64	9500
Density of Air, ρ air = 0.00122 g/cc at 15.6 °C							
°API Gravity of Condensate = 31.86°							
Gas-Condensate ratio = 142260							
Gas Constant, R = 8.3145							
Specific gravity of Gas, G = 0.5624							

Data source: Geology Division, Bangladesh Petroleum Exploration and Production Company Limited, Dhaka

Table 3. *Calculated Values for Batzle and Wang Model (for varying saturation with constant pressure).*

Calculation For New Gas Zone III			
Properties	Gas	Brine	Mixture
Density, g/cc	0.1151	1.002	0.523
Acoustic Velocity, m/s	526.3145	1574.348	334.1256
Bulk Modulus, Mpa	31.8754	2483.332	58.3901
Calculation For New Gas Zone II			
Properties	Gas	Brine	Mixture
Density, g/cc	0.1346	1.0022	0.6899
Acoustic Velocity, m/s	546.9245	1586.719	397.0967
Bulk Modulus, MPa	40.2731	2523.198	108.7831

546.92 m/s, and 40.27 MPa, respectively, for gas phase (Table 5). For brine and mixture phase, all the parameters (density, acoustic velocity and bulk modulus) have changed significantly (Table 3).

The cross-plot between bulk modulus and density for changing the saturation of gas zones have been formulated which are given in Fig 3a-b. The values of modulus and density for changing saturation are also listed in table 4.

Usually, saturations of gas zones usually change from the initial condition within creasing production. In Fig. 3a-b, the red marked position is the initial condition, whereas the green line indicates the production direction. These Figs show that for saturation changes with constant pressure, both the bulk modulus and density increases as the water saturation increases. However, the density increases very rapidly and bulk modulus increases slowly at the initial stage of production, whereas reverse situation (density increases slowly and bulk modulus increases very rapidly) exists at the later stage.

4.1.2. Gassmann-Biot model

Table 5 and 6demonstrate the use of the Gassmann-Biot equations with fluid and rock properties to determine the overall reservoir rock seismic properties such as velocity and density. The input values include porosity (ρ), solid material bulk modulus (Ks) and density (ρs), brine density (ρ_w), bulk modulus (K_w), hydrocarbon density (ρ_{hyd}) and bulk modulus (K_{hyd}). The important output values are the bulk density (ρ_d), P-wave velocity (V_p), S-wave velocity (V_s), acoustic impedance (AI), and Poisson's ratio (σ) as they vary due to changes in saturation. The dry frame modulus is held constant.

Using the Gassmann-Biot model at the reservoir condition, we found that the values of dry frame rigidity (G) are 5.67431 and 5.21752 GPA, bulk density (ρ) are 2.19997 and 2.20135 g/cm^3, fluid bulk modulus (K_f) are 0.05838 and 0.108784 GPA, saturated bulk modulus (KB) are 33.9173 and 16.33908 GPA, compressional wave velocity (V_p) are 4342.36 and 3253.07 m/s, shear wave velocity (V_s) are 1606.00 m/s and 1539.526 m/s for New Gas Zone III and II, respectively (Table 6). Some other

Table 4. *Modulus and density for different saturation condition.*

Modulus-Density for Saturation Change							
Gas and Brine (New Gas Zone III)				Gas and Brine (New Gas Zone II)			
Gas %	Brine %	Density, g/cc	Modulus, Gpa	Gas %	Brine %	Density, g/cc	Modulus, Gpa
5	95	0.958	0.5125	5	95	0.959	0.618
10	90	0.913	0.2857	10	90	0.915	0.3521
20	80	0.825	0.1516	20	80	0.829	0.1893
30	70	0.736	0.1032	30	70	0.742	0.1294
40	60	0.647	0.0782	40	60	0.655	0.0983
50	50	0.558	0.0629	50	50	0.568	0.0793
60	40	0.469	0.0527	60	40	0.482	0.0664
70	30	0.381	0.0453	70	30	0.393	0.0571
80	20	0.292	0.0397	80	20	0.308	0.0501
90	10	0.204	0.0354	90	10	0.221	0.0447

Table 5. *Input values of Gassmann-Biot model (for varying saturation with constant pressure).*

Input Parameter	New Gas Zone III	New Gas Zone II
Depth (m)	1656-1680	1992-2017
Pressure (MPa)	16.3888	19.7328
Temperature (°C)	46.67	51.11
Solid Material Bulk Modulus (Gpa)	30	30
Solid Material Density (g/cc)	2.8297	2.4577
Water Bulk Modulus (K_W)	2.483332 GPa	2.523198 GPa
Water Density (ρ_w)	1.002 g/cc	1.0021 g/cc
Hydrocarbon Balk Modulus (K_{hyd})	0.031875 Gpa	0.040273 Gpa
Hydrocarbon Density (ρ_{hyd})	0.115 g/cc	0.1346 g/cc
Logged P-wave velocity (V_{pi})	2650 m/s	2540 m/s
Logged S-wave velocity (V_{si})	1606 m/s	1540 m/s
Logged Bulk Density (ρ_{bi})	2.2 g/cc	2.2 g/cc
Fluid Bulk Modulus at logged condition (K_{fi})	0.5839 Gpa	1.0878 Gpa

Values of output parameters for different saturation are listed in Table 6.

Subsequently, we have assumed full water (wet) and gas saturation is 95% water and 90% gas respectively. We also considered the irreducible gas saturation or depleted reservoir condition at 20% gas or 80% water (Fig. 6-7).

Based on the hypothesis on pore fluid distribution in pore space, it is concluded that pore fluid should increase compressional velocity and decrease slightly shear velocity of the rocks [2,3]. Moreover, experimental results also show that compressional and shear velocity are related to saturation [23,24]. Gregory [25] opined that saturation has larger effect on rock velocities in low porosity rocks than that in high porosity rocks. V_P in fully water-saturated rocks is obviously larger than those in partially water-saturated rocks. V_S do not always decrease with the increase of saturation. Instead V_S is associated with pressure, porosity and the chemical interactions between pore fluid and rock skeleton. Our modeling result also shows (Fig. 3c-d) the compressional velocity (V_p, blue curve) increases with the increasing water saturation. The compressional wave velocity (V_p, blue curve) trends from 6098 m/s (20000 ft/s) and 4123 m/s (13527 ft/s) at full water saturation to 3860 m/ s (12664 ft/s) and2730 m/ s (8957 ft/s) at full gas saturation for New Gas Zone III and II, respectively.

At reservoir conditions, during production the water saturation varies from water saturation 46% to 80% and 64% to 80% for New Gas Zone III and II, respectively. Within this saturation range a significant variations has been found in the compressional velocity (21.5% and 10.2% for New Gas Zone III and II, respectively (Table 6).

The Figs. 4a-b and 4e-f show that the bulk density and PR increase linearly with the increase of water saturation. The bulk density (ρ) trends from 2.31863 and 2.24034 g/cm^3 at full water saturation to 2.11280 and 2.13342 g/cm^3 at full gas saturation for New Gas Zone III and II, respectively. The bulk density (blue line in Fig. 4a-b) increases from 2.1999 and 2.201 g/cm^3 to 2.282 and 2.221 g/cm^3, respectively for New Gas Zone III and II with the water saturation increases from reservoir condition to irreducible gas saturation (20% gas). Similarly, for New Gas Zone III and IIPR (blue line in Figs. 4e-f) values are trending from 0.465 and 0.421 at full water saturation to 0.390 and 0.255 at full gas saturation for New Gas Zone III and II, respectively. The acoustic impedance (blue line in Figs. 4c-d) values are increased with the increasing water saturation. The properties of the pore fluids have amplitude variation with offset at the interface between the overlying shale and the reservoir [11]. The acoustic impedance values are trending from 14140 and 9237 m/s*g/cm^{3}at full water saturation to 8156.221and 5823.6798m/s*g/cm^3 at full gas saturation for New Gas Zone III and II, respectively. The point labeled (green mark) reservoir conditions in Fig. 5 is related to point labeled (red mark) in Fig. 3a-b. If the water saturation increases, the fluid bulk modulus and density increase, according to the green marked direction in Figs. 3a-b, it has an increasing effect on PR and the acoustic impedance, and it can clearly identify from Figs. 5a-d is a cross-plot of the compressional velocity of a compressional wave passing through the fluid and rock matrix versus the bulk density. These Figs. show the changes in velocity and density values as the reservoir becomes increasingly water saturated. It is easily recognizable from the Fig. 5c-d that compressional wave velocity and bulk density increases as water saturation increases. However, the Figs. 5e-f is a cross-plot of shear wave velocity versus compressional wave velocity is consistent with the finding of Batzle and Wang model (Fig. 3c-d).

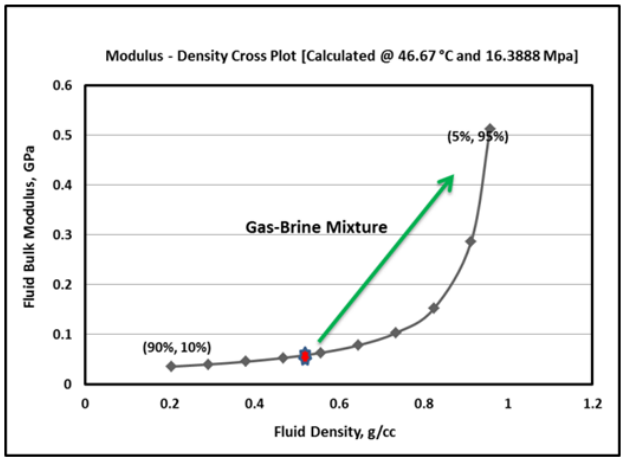

a.

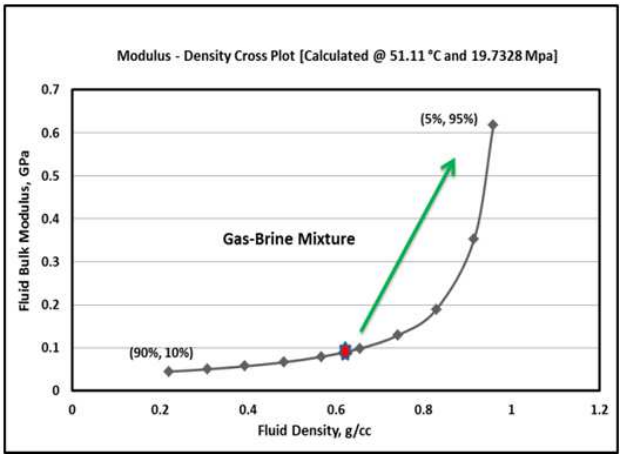

b.

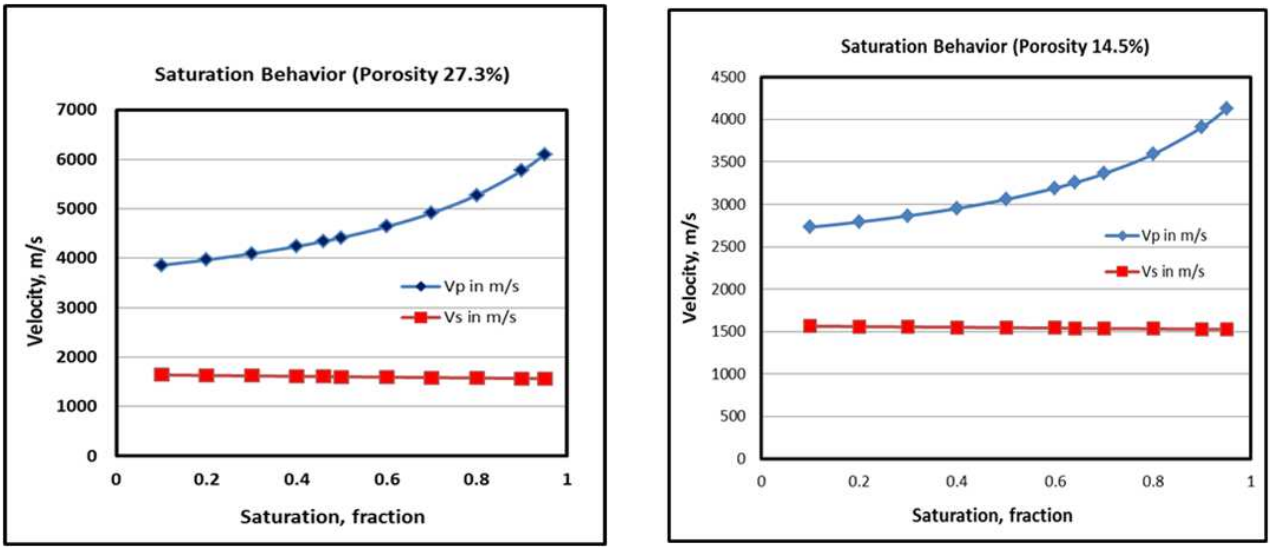

c. d.

Fig. 3. *Cross-plot of fluid modulus and density as saturation values change (gas%, brine %) for a) New Gas Zone III and b) New Gas Zone II. Velocity versus saturation shows how water saturation affects a two phase mixture of gas and brine in a sandstone matrix from water to gas saturated conditions for c) New Gas Zone III and d) New Gas Zone II.*

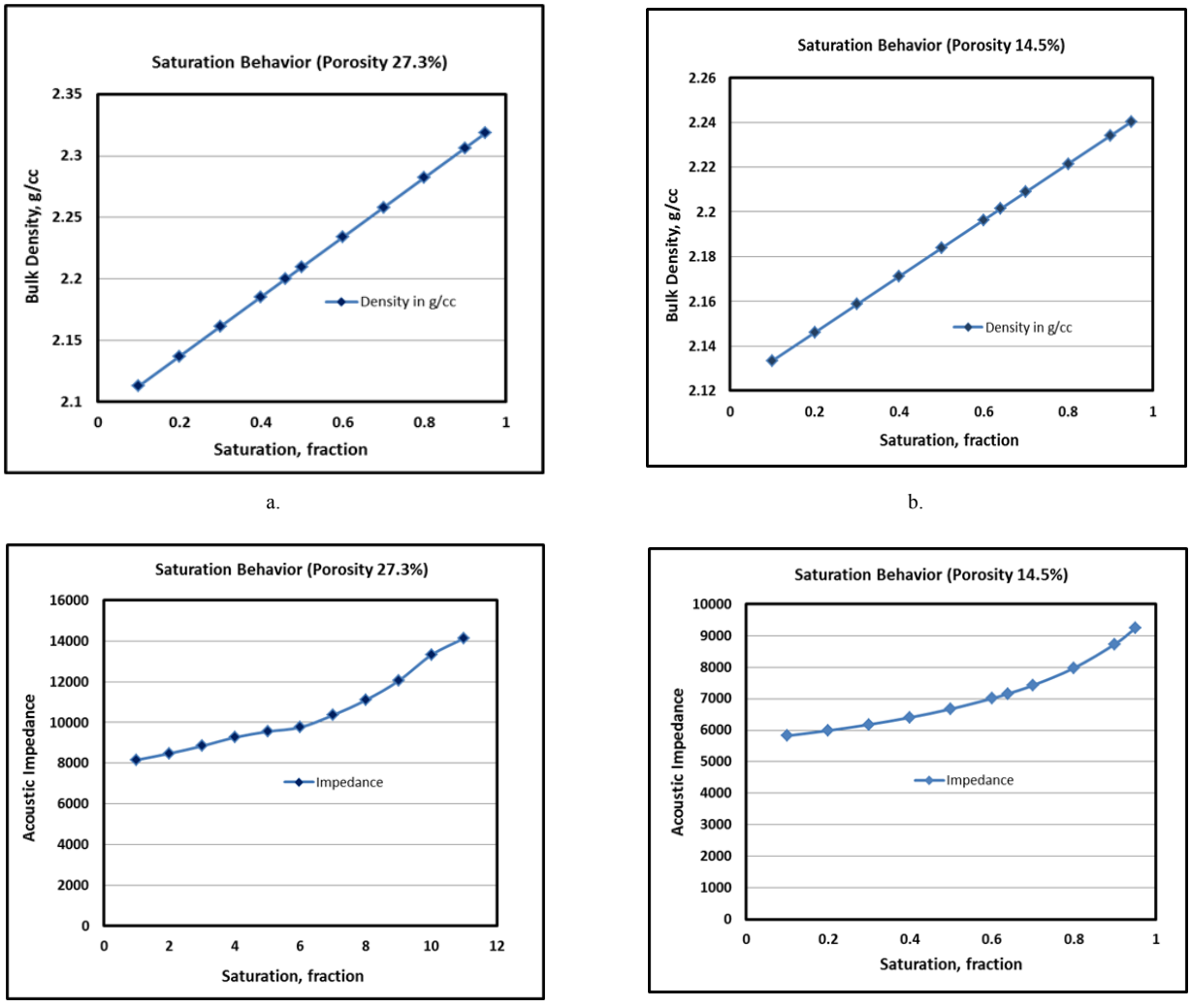

a. b.

c. d.

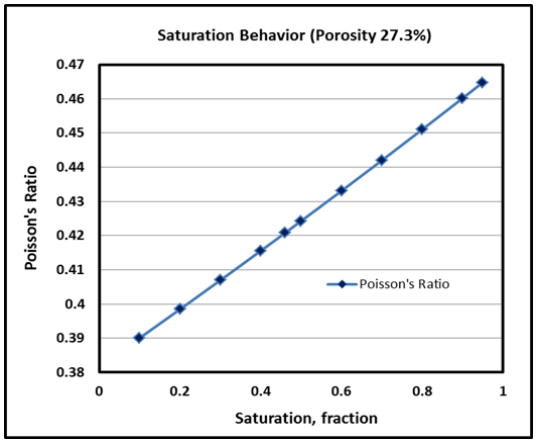

e.

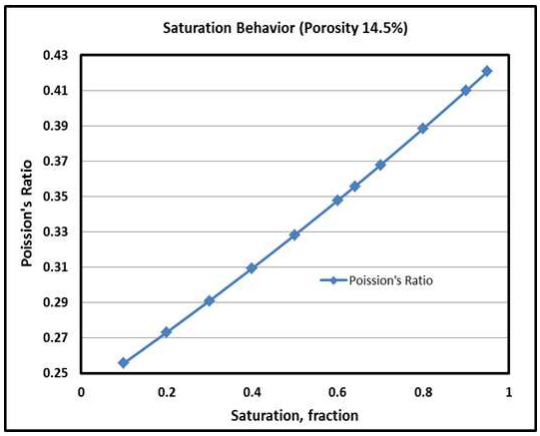

f.

Fig. 4. *Bulk density versus saturation for a) New Gas Zone III and b) New Gas Zone II, Acoustic Impedance versus saturation for c) New Gas Zone III and d) New Gas Zone II, and Poisson's ratio versus saturation for e) New Gas Zone III and f) New Gas Zone II shows how water saturation affects a two phase mixture of gas and brine in a sandstone matrix from water to gas saturated conditions.*

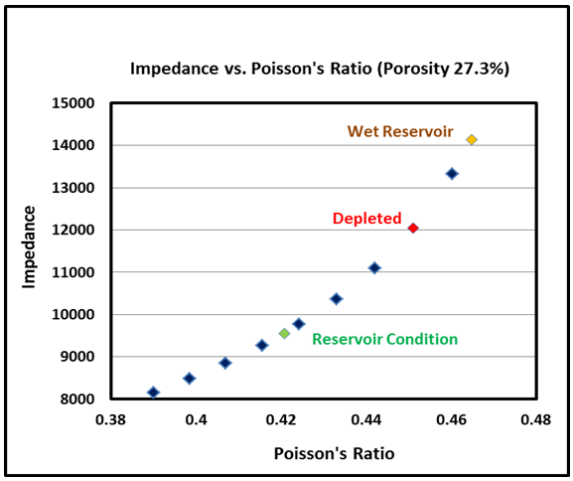

a.

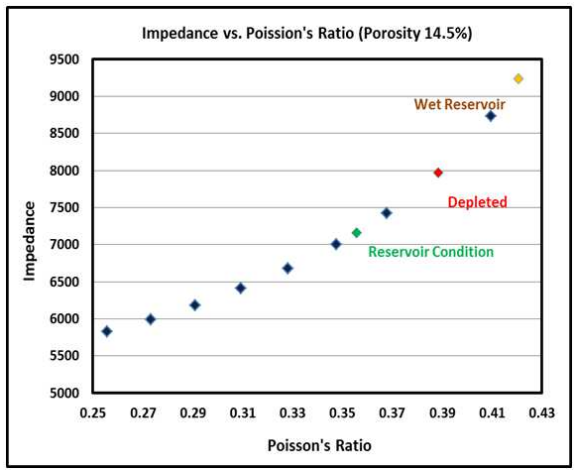

b.

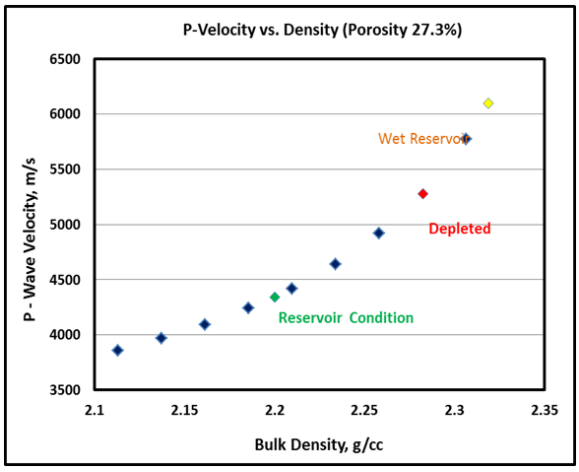

c.

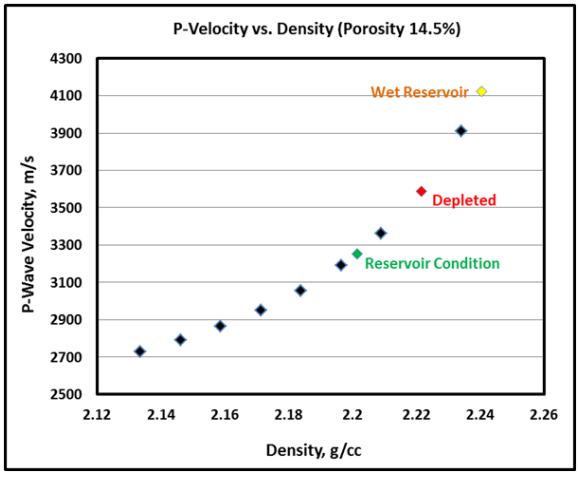

d.

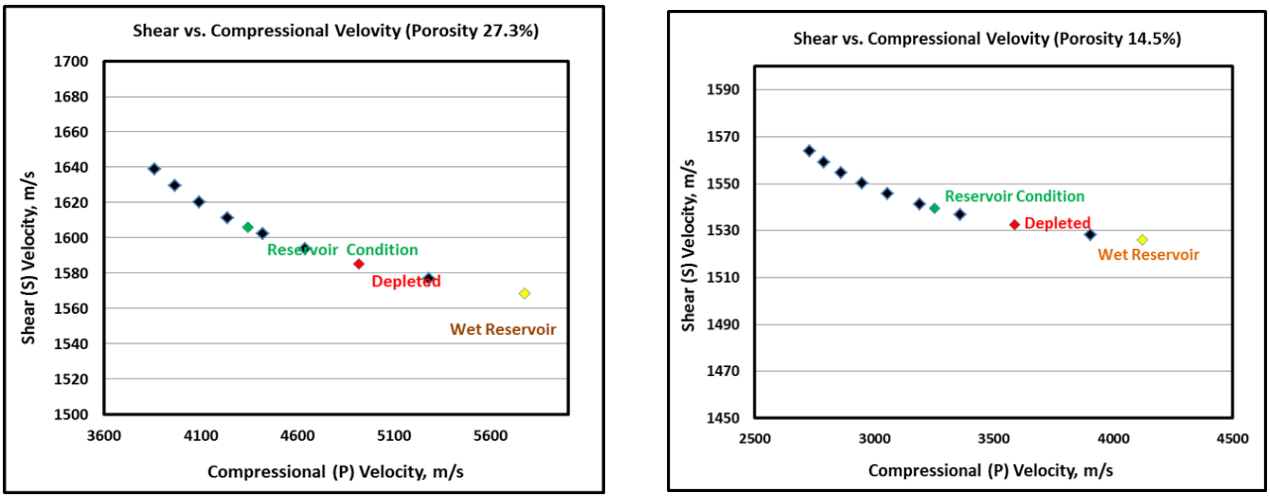

e. f.

Fig. 5. *Acoustic impedance Vs. Poisson's ratio cross-plot for a) New Gas Zone III and b) New Gas Zone II, Compressional wave velocity Vs. Bulk density cross-plot for c) New Gas Zone III and d) New Gas Zone II, and Shear wave velocity Vs. Compressional wave velocity cross-plot for e) New Gas Zone III and f) New Gas Zone II for a two phase mixture of gas and brine in a sandstone matrix from water to gas saturated conditions.*

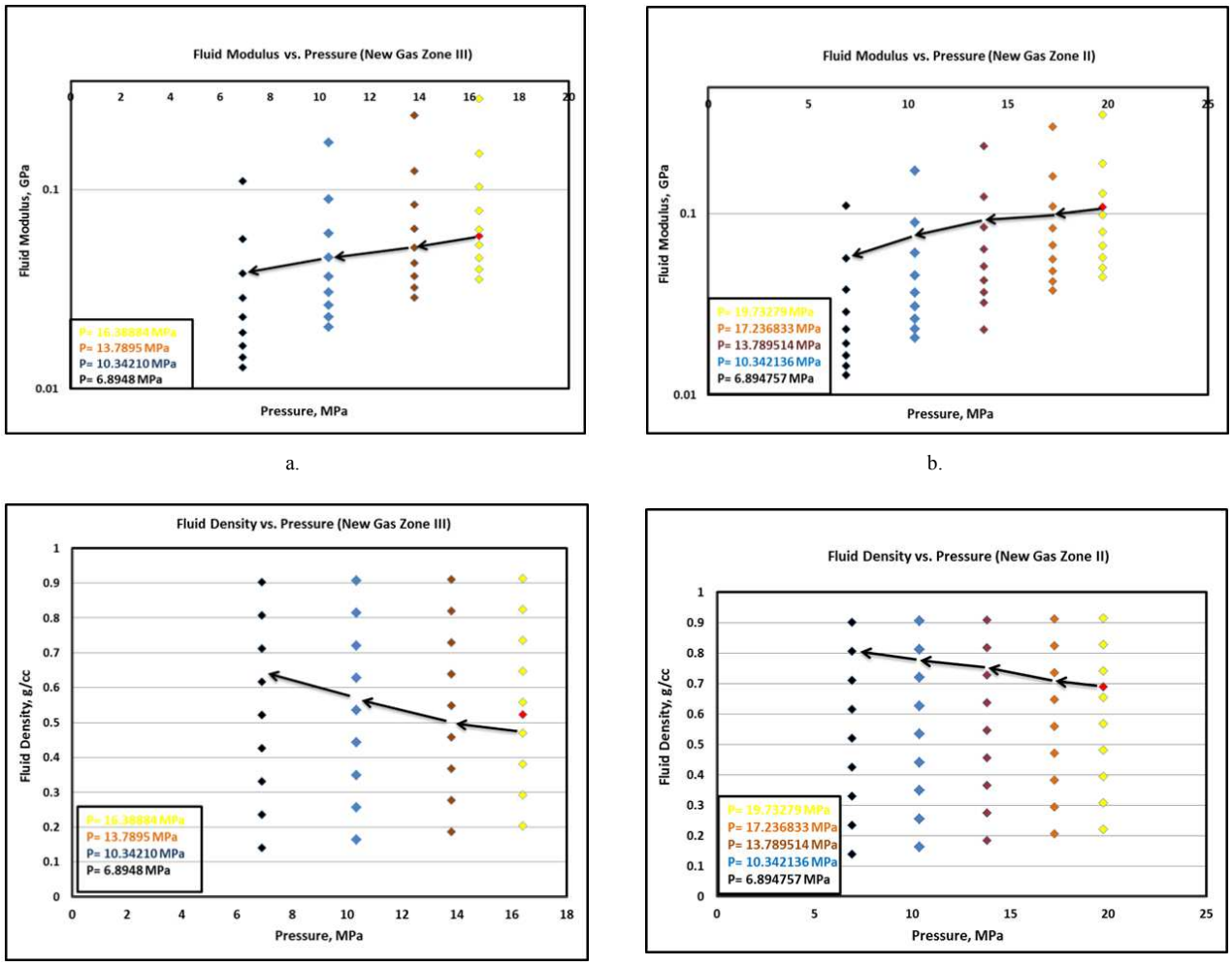

a. b.

c. d.

Fig. 6. *Fluid modulus versus pressure shows the changes in the fluid modulus as the pressure and saturation in the reservoir changes during production for a) New Gas Zone III and b) New Gas Zone II. Fluid density versus pressure shows the changes in the fluid density as the pressure and saturation in the reservoir changes during production for c) New Gas Zone III and d) New Gas Zone II.*

4.2. Fluid Models for Varying Saturation and Pressure

4.2.1. Batzle and Wang Model

Here we considered gas saturation would change from 90% to 10% of reservoir pressure of 2000 psi, 1500 psi and 1000 psi pressure for New Gas Zone III and at reservoir pressure of 2500 psi, 2000 psi, 1500 psi and 1000 psi for New Gas Zone II. The moduli and densities for different saturation and pressure were calculated from this model are listed (Table 7). The cross plot between fluid modulus and density versus pressure shows that the fluids have a wide range of fluid moduli and densities of different saturation conditions (Fig. 6). The different fluid moduli and densities for the initial reservoir pressure conditions are shown by the yellow diamonds. In this line the red diamond indicates the initial saturation point. The light brown diamond series is for 17.236893 MPa (2500 psi), dark brown series is for3.789514 MPa (2000 psi), blue diamond series is for 10.342136 MPa (1500 psi) and the last black diamond series is for 6.894757 MPa (1000 psi) pressure. For New Gas Zone III, we assumed that during production fluid saturations (Gas: Brine) would (0.54: 0.46), (0.50: 0.50), (0.40: 0.60) and (0.30: 0.70) at 16.38884 MPa (2377 psi), 13.789514 MPa (2000 psi), 10.342136 MPa (1500 psi) and 6.894757 MPa (1000 psi) pressure, respectively. Similarly, for New Gas Zone II we also assumed that during production fluid saturations (Gas: Brine) would (0.36: 0.64), (0.32: 0.68), (0.28: 0.72), (0.24: 0.76) and (0.20: 0.80) at 19.737279 MPa (2862 psi), 17.236893 MPa (2500 psi), 13.789514 MPa (2000 psi), 10.342136 MPa (1500 psi) and 6.894757 MPa (1000 psi) pressure, respectively. The dry frame modulus is held constant. Figs. 6a-b is showing the predicted fluid modulus path versus pressure. The black connecting line with arrow head shows the downward curve for the decreasing value of fluid modulus with respect to pressure fall during production. The fluid modulus increases with water saturation at a constant pressure, but decreases with pressure fall and overall it decreases through the assumed production path. So, the effect of pressure fall is dominating here for fluid modulus changes.

Table 6. *Calculated values of Gassmann-Biot model (for varying saturation with constant pressure).*

Zones	Water Saturation, ρ_w	Dry Frame Rigidity, G	Bulk Density, g/cm^3	Fluid Bulk Modulus, K_f	Saturated Bulk Modulus, K_b	P-Wave Velocity, V_p	S-Wave Velocity, V_s	Poisson's Ratio, σ	Acoustic impedance, AI
New Gas Zone III	0.1	5.67431	2.11280	0.03536	23.9203	3860.38	1638.80	0.39008	8156.221
	0.2	5.67431	2.13701	0.03971	26.0534	3966.33	1629.49	0.39847	8476.134
	0.3	5.67431	2.16123	0.04528	28.6042	4090.94	1620.34	0.40696	8841.479
	0.4	5.67431	2.18544	0.05267	31.7087	4239.21	1611.33	0.41556	9264.569
	0.46	5.67431	2.19997	0.05838	33.9173	4342.36	1606.00	0.42076	9553.107
	0.5	5.67431	2.20966	0.06294	35.5690	4418.25	1602.48	0.42426	9762.856
	0.6	5.67431	2.23387	0.07818	40.4996	4638.59	1593.77	0.43307	10362.06
	0.7	5.67431	2.25809	0.10316	47.0172	4916.51	1585.20	0.44199	11101.95
	0.8	5.67431	2.28230	0.15159	56.0348	5278.9	1576.77	0.45102	12048.07
	0.9	5.67431	2.30652	0.28574	69.3323	5774.02	1568.47	0.46016	13317.93
	0.95	5.67431	2.31863	0.51251	78.6664	6098.44	1564.37	0.46478	14140.03
New Gas Zone II	0.1	5.21752	2.13342	0.044669	8.940381	2729.727	1563.842	0.255723	5823.6798
	0.2	5.21752	2.14600	0.050141	9.758707	2790.889	1559.252	0.273109	5989.2691
	0.3	5.21752	2.15858	0.057142	10.74193	2863.418	1554.703	0.290983	6180.9366
	0.4	5.21752	2.17116	0.066415	11.94548	2950.592	1550.192	0.309366	6406.2241
	0.5	5.21752	2.18374	0.079281	13.45275	3057.135	1545.721	0.32828	6676.0001
	0.6	5.21752	2.19632	0.098329	15.39533	3190.143	1541.289	0.347748	7006.5846
	0.64	5.21752	2.20135	0.108784	16.33908	3253.07	1539.526	0.355696	7161.1596
	0.7	5.21752	2.20890	0.129425	17.99361	3360.853	1536.894	0.367795	7423.7942
	0.8	5.21752	2.22148	0.189284	21.64697	3588.306	1532.536	0.388448	7971.3515
	0.9	5.21752	2.23405	0.352158	27.16182	3907.938	1528.216	0.409735	8730.5641
	0.95	5.21752	2.24034	0.618079	31.12681	4122.973	1526.069	0.420624	9236.8976

However, a reverse condition has been seen from the Figs. 6c-d, which indicates that the fluid density of the reservoir is not affected as strongly as the modulus by pressure changes and variations of saturation. The density is increasing with the increase of water saturation and decreases with pressure fall for both gas zones.

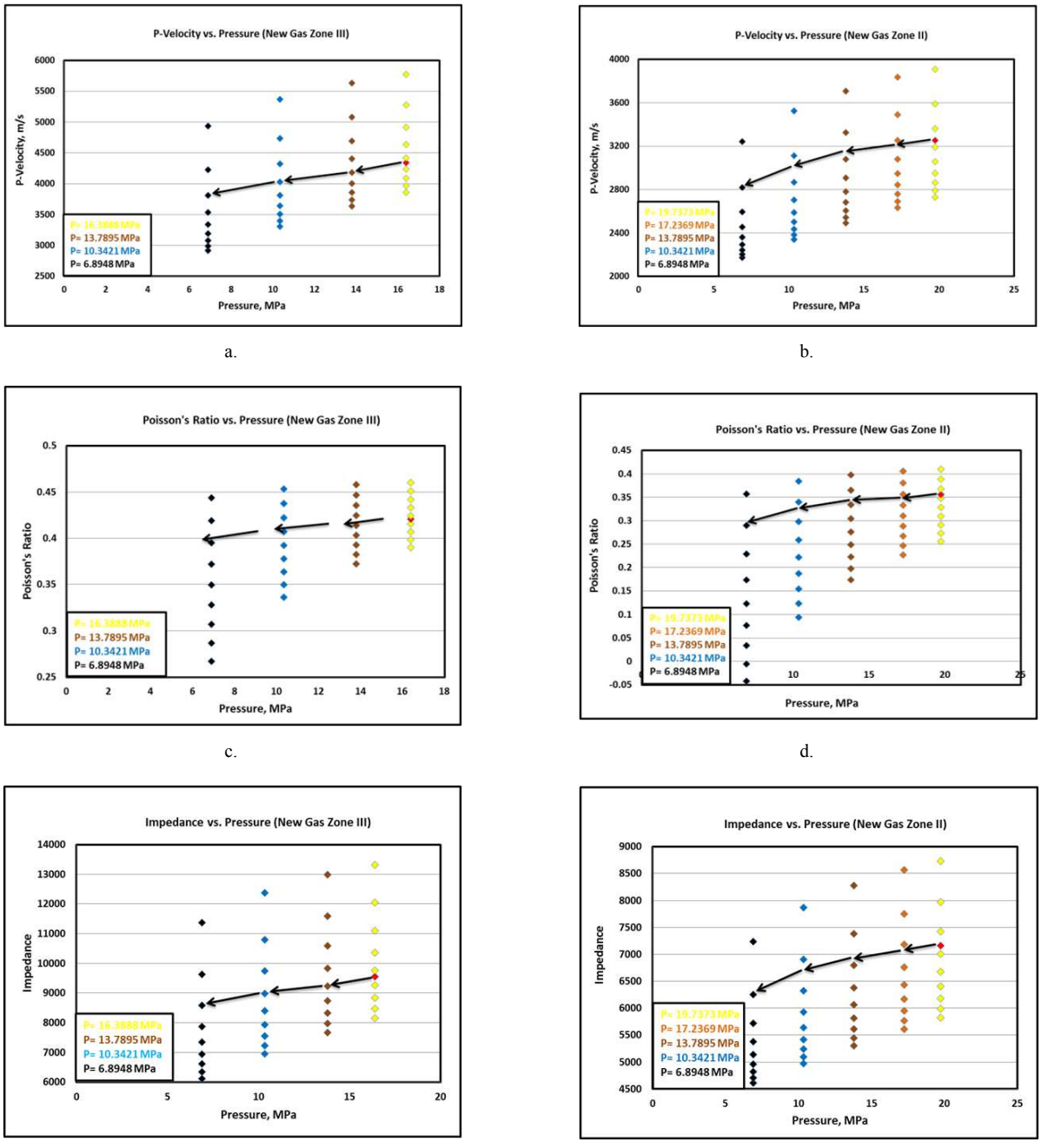

Fig. 7. *P-wave velocity versus pressure shows how the velocity changes as the pressure and saturation in the reservoir changes for a) New Gas Zone III and b) New Gas Zone II. The Poisson's ratio versus pressure shows how the velocity changes as the pressure and saturation in the reservoir changes for c) New Gas Zone III and d) New Gas Zone II. Acoustic impedance versus pressure shows how the Poisson's ratio changes as the pressure and saturation in the reservoir changes for e) New Gas Zone III and f) New Gas Zone II.*

Table 7. *Calculated fluid properties from Batzle and Wang Model (for varying saturation and pressure).*

Calculation for New Gas Zone III							
Pressure: 16.38884 Mpa (2377 psi)				Pressure: 13.7895 Mpa (2000 psi)			
Density of Gas: 0.115 g/cc				Density of Gas: 0.0963 g/cc			
Modulus of Gas: 0.031754 Gpa				Modulus of Gas: 0.025795 Gpa			
Density of Brine: 1.0019 g/cc				Density of Brine: 1.0008 g/cc			
Modulus of Brine: 2.483332 Gpa				Modulus of Brine: 2.466893 Gpa			
Gas %	Brine %	Density, g/cc	Modulus, Gpa	Gas %	Brine %	Density, g/cc	Modulus, Gpa
90	10	0.2038	0.035367	90	10	0.1868	0.028627
80	20	0.2924	0.039717	80	20	0.2772	0.032159
70	30	0.3811	0.045287	70	30	0.3677	0.036685

Calculation for New Gas Zone III							
60	40	0.4698	0.052675	60	40	0.4581	0.042693
54	46	0.523	0.05839	50	50	0.5486	0.051055
50	50	0.5585	0.062943	40	60	0.639	0.063491
40	60	0.6472	0.078183	30	70	0.7295	0.083934
30	70	0.7359	0.103162	20	80	0.8199	0.123795
20	80	0.8246	0.151594	10	90	0.9104	0.235759
10	90	0.9132	0.285744				
Pressure: 10.3421 Mpa (1500 psi)				Pressure: 6.8948 Mpa (1000 psi)			
Density of Gas: 0.0707 g/cc				Density of Gas: 0.0454 g/cc			
Modulus of Gas: 0.018361 Gpa				Modulus of Gas: 0.011486 Gpa			
Density of Brine: 0.9994 g/cc				Density of Brine: 0.9979 g/cc			
Modulus of Brine: 2.445394 Gpa				Modulus of Brine: 2.424272 Gpa			
Gas %	Brine %	Density, g/cc	Modulus, Gpa	Gas %	Brine %	Density, g/cc	Modulus, Gpa
90	10	0.1636	0.020384	90	10	0.1407	0.012756
80	20	0.2563	0.022909	80	20	0.2359	0.014341
70	30	0.3493	0.026146	70	30	0.3312	0.016375
60	40	0.4422	0.030449	60	40	0.4264	0.019083
50	50	0.5351	0.036449	50	50	0.5217	0.022864
40	60	0.6279	0.045392	40	60	0.6169	0.028512
30	70	0.7208	0.06015	30	70	0.7122	0.037868
20	80	0.8137	0.089129	20	80	0.8075	0.056362
10	90	0.9065	0.171989	10	90	0.9027	0.110163
Calculation for New Gas Zone II							
Pressure: 19.73279 Mpa (2862 psi)				Pressure: 17.236893 Mpa(2500 psi)			
Density of Gas: 0.1346 g/c				Density of Gas: 0.1182 g/cc			
Modulus of Gas: 0.040273 Gpa				Modulus of Gas: 0.033909 Gpa			
Density of Brine: 1.0022 g/cc				Density of Brine: 1.0012 g/cc			
Modulus of Brine: 2.523198 Gpa				Modulus of Brine: 2.506883 Gpa			
Gas %	Brine %	Density, g/cc	Modulus, Gpa	Gas %	Brine %	Density, g/cc	Modulus, Gpa
90	10	0.2214	0.044669	90	10	0.2065	0.037621
80	20	0.3081	0.050141	80	20	0.2948	0.042244
70	30	0.3949	0.057142	70	30	0.3831	0.048163
60	40	0.4817	0.066415	60	40	0.4714	0.056011
50	50	0.5684	0.079281	50	50	0.5597	0.066915
40	60	0.6552	0.098329	40	60	0.6479	0.083089
36	64	0.6899	0.108783	30	70	0.7363	0.109574
30	70	0.7419	0.129424	20	80	0.8246	0.160846
20	80	0.8286	0.189281	10	90	0.9129	0.302297
10	90	0.9154	0.352146				
Pressure: 13.789514 Mpa(2000 psi)				Pressure: 10.342136 Mpa(1500 psi)			
Density of Gas: 0.0941 g/cc				Density of Gas: 0.0692 g/cc			
Modulus of Gas: 0.025843 Gpa				Modulus of Gas: 0.018437 Gpa			
Density of Brine: 0.9998 g/cc				Density of Brine: 0.9983 g/cc			
Modulus of Brine: 2.484589 Gpa				Modulus of Brine: 2.462607 Gpa			
Gas %	Brine %	Density, g/cc	Modulus, Gpa	Gas %	Brine %	Density, g/cc	Modulus, Gpa
90	10	0.1847	0.022868	90	10	0.1621	0.020469
80	20	0.2752	0.032219	80	20	0.255	0.023004
70	30	0.3658	0.036764	70	30	0.3479	0.026255
60	40	0.4564	0.042774	60	40	0.4408	0.030576
50	50	0.5469	0.051153	50	50	0.5338	0.036601
40	60	0.6375	0.063614	40	60	0.6267	0.045582
30	70	0.7281	0.084101	30	70	0.7196	0.060403
20	80	0.8186	0.124052	20	80	0.8125	0.089507
10	90	0.9092	0.236305	10	90	0.9054	0.172735
Pressure: 6.894757 Mpa(1000 psi)							
Density of Gas: 0.0445 g/cc				Density of Brine: 0.9969 g/cc			
Modulus of Gas: 0.011539 Gpa				Modulus of Brine: 2.440969 Gpa			
Gas %		Brine %		Density, g/cc		Modulus, Gpa	
90		10		0.1397		0.012815	
80		20		0.2349		0.014408	
70		30		0.3302		0.016452	
60		40		0.4255		0.019172	
50		50		0.5207		0.022971	
40		60		0.6159		0.028646	
30		70		0.7112		0.038046	
20		80		0.8064		0.056628	
10		90		0.9017		0.110688	

4.2.2. Gassmann-Biot Model

The initial conditions of the Figs. are same as the Fig. 6. Biot-Gassmann theory accurately predicts velocity ratios with respect to differential pressure for given porosity. However, because the velocity ratio is weakly related to porosity, it is not appropriate to investigate the velocity ratio with respect to porosity (φ). The velocity ratio has been used for many purposes, such as a lithology indicator, determining degree of consolidation, identifying pore fluid, and predicting velocities [27]. The velocity ratio usually depends on porosity, degree of consolidation, clay content, differential pressure, pore geometry, and other factors. The velocity ratio for dry rock or gas-saturated rock is almost a constant irrespective of porosity and differential pressure, whereas the velocity ratio of wet rock depends significantly on porosity and differential pressure. P-wave to S-wave velocity ratio (V_p/V_s) for the both gas zones Fenchuganj Gas Field show value of more than 2.0 which indicate the presence of gas in the unconsolidated rock [28] with higher porosity [29].

Fig. 7 shows the predicted P-wave velocity, PR and acoustic impedances under differential pressure due to gas production increases. The black connecting line with arrow head shows the downward curve for the decreasing value of all parameters respects to pressure fall during production. These parameters increases with water saturation at a constant pressure, but decreases with pressure fall. So, it can forecast that the New Gas Zone II has greater effect on parameters change than the New Gas Zone III.

4.3. AVO Analysis

In this section, we determined and analyzed the AVO response for New Gas Zone III and II of Fenchuganj Gas Field. Firstly, we took assumptions given by Shuey [21] (1985) and interpreted AVO using Zoeppritz (1919) equation for 0-30° incident angle.

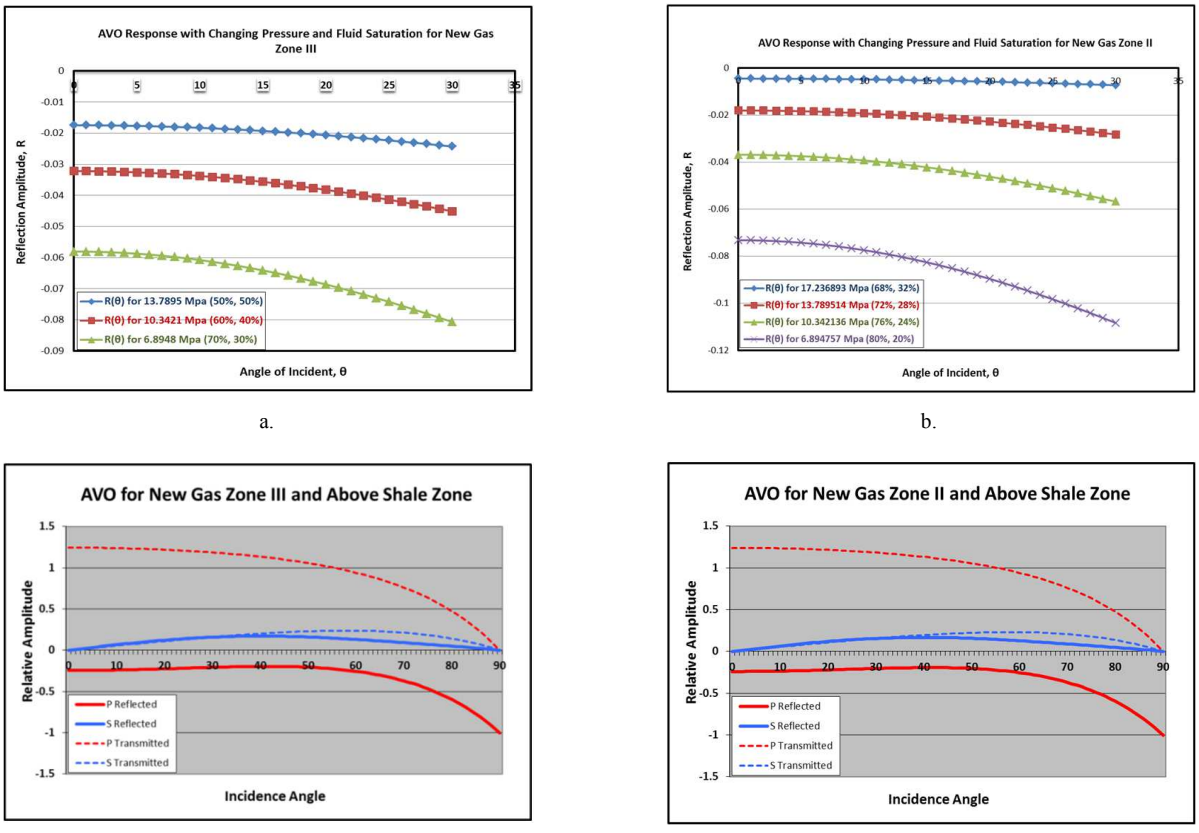

Fig. 8. *Reflection amplitude versus offset shows the AVO between a definite pressure-saturation condition and reservoir condition for a) New Gas Zone III and b) New Gas Zone II. Reflection amplitude versus offset shows the AVO between a) New Gas Zone III and above shale zone, and b) New Gas Zone II and above shale zone.*

The input values (Vp, ρ_b and σ) for AVO interpretation are taken from the output values (Table 8) of Gassmann-Biot model for varying saturation and pressure. Every reflection curve of Figs. 8a-b represents the comparison of seismic reflection change due to change of pressure and saturation of a definite layer from the reservoir condition. It is obvious that the AVO response decreases as water saturation increases.

Secondly, we have interpreted AVO without any assumptions. We used full Zoeppritz [1] equation with the help of an AVO calculator by Timothy et al. which starts with negative values and decreases with the offset

indicating of low impedance gas sand class 3 AVO [11]. This characteristic of AVO indicates bright zone that is potential for hydrocarbon zone [11].

Table 8. *Calculated fluid and rock properties from Gassmann-Biot Model (for varying saturation and pressure).*

Calculation for New Gas Zone III						
Input Parameters (Fixed)				Symbol	Value	Unit
Depth				D	1656-1680	m
Temperature				T	46.67	°C
Solid Material Bulk Modulus				K_s	30	Gpa
Solid Material Density				ρ_s	2.8297	g/cc
Logged P-wave velocity				V_{pi}	2650	m/s
Logged S-wave velocity				V_{si}	1606	m/s
Logged Bulk Density				ρ_{bi}	2.2	g/cc
Fluid Bulk Modulus at logged condition				K_{fi}	0.5839	Gpa
Parameter (Variable)				Symbol	Value	Unit
Pressure				P	16.3884	Mpa
Water Bulk Modulus				K_w	2.483332	GPa
Water Density				ρ_w	1.0019	g/cc
Hydrocarbon Bulk Modulus				K_{hyd}	0.031754	Gpa
Hydrocarbon Density				ρ_{hyd}	0.115	g/cc
S_w	S_g	ρ_b in g/cc	V_p in m/s	V_s in m/s	σ	AI
0.1	0.9	2.11279927	3860.397409	1638.80682	0.39008381	8156.24483
0.2	0.8	2.13701164	3966.357727	1629.49652	0.39847393	8476.15263
0.3	0.7	2.16122401	4090.965635	1620.34312	0.40696595	8841.49315
0.4	0.6	2.18543638	4239.234444	1611.34226	0.41556172	9264.57718
0.46	0.54	2.1999638	4342.39474	1606.01321	0.42076978	9553.11124
0.5	0.5	2.20964875	4418.284777	1602.48975	0.42426317	9762.85743
0.6	0.4	2.23386112	4638.628155	1593.78156	0.43307226	10362.0511
0.7	0.3	2.25807349	4916.552911	1585.2138	0.44199099	11101.9378
0.8	0.2	2.28228586	5278.937105	1576.78276	0.45102143	12048.0435
0.9	0.1	2.30649823	5774.067549	1568.48482	0.46016568	13317.8766
Parameter (Variable)				Symbol	Value	Unit
Pressure				P	13.7895	Mpa
Water Bulk Modulus				Kw	2.466893	GPa
Water Density				ρw	1.0008	g/cc
Hydrocarbon Balk Modulus				K hyd	0.025795	Gpa
Hydrocarbon Density				ρ hyd	0.0963	g/cc
Sw	Sg	ρb in g/cc	Vp in m/s	Vs in m/s	σ	AI
0.1	0.9	2.10817465	3638.34716	1640.60333	0.37238851	7670.27125
0.2	0.8	2.1328675	3739.577122	1631.0788	0.38253207	7976.02251
0.3	0.7	2.15756035	3860.010094	1621.71825	0.3928267	8328.20473
0.4	0.6	2.1822532	4005.19392	1612.51704	0.40327579	8740.34725
0.5	0.5	2.20694605	4183.197791	1603.47068	0.41388284	9232.09184
0.6	0.4	2.2316389	4406.28949	1594.57489	0.42465147	9833.24703
0.7	0.3	2.25633175	4694.207908	1585.82553	0.43558538	10591.6903
0.8	0.2	2.2810246	5081.196991	1577.21862	0.44668843	11590.3353
0.9	0.1	2.30571745	5633.260806	1568.75036	0.45796456	12988.7077
Parameter (Variable)				Symbol	Value	Unit
Pressure				P	10.3421	Mpa
Water Bulk Modulus				Kw	2.445394	GPa
Water Density				ρw	0.9994	g/cc
Hydrocarbon Balk Modulus				K hyd	0.018361	Gpa
Hydrocarbon Density				ρ hyd	0.0707	g/cc
Sw	Sg	ρb in g/cc	Vp in m/s	Vs in m/s	σ	AI
0.1	0.9	2.10184651	3308.279078	1643.0712	0.33628418	6953.49483
0.2	0.8	2.12720002	3398.769408	1633.25019	0.34987236	7229.86235
0.3	0.7	2.15255353	3508.428829	1623.60321	0.36373972	7552.08086
0.4	0.6	2.17790704	3643.361622	1614.12518	0.37789496	7934.90293
0.5	0.5	2.20326055	3812.755286	1604.81122	0.39234714	8400.49331
0.6	0.4	2.22861406	4031.192373	1595.65666	0.40710569	8983.972

Calculation for New Gas Zone III						
0.7	0.3	2.25396757	4323.493664	1586.65699	0.42218046	9745.01451
0.8	0.2	2.27932108	4736.177418	1577.80791	0.43758173	10795.269
0.9	0.1	2.30467459	5369.75109	1569.10525	0.45332021	12375.5289
Parameter (Variable)				Symbol	Value	Unit
Pressure				P	6.8948	Mpa
Water Bulk Modulus				Kw	2.424272	GPa
Water Density				ρw	0.9979	g/cc
Hydrocarbon Balk Modulus				K hyd	0.011486	Gpa
Hydrocarbon Density				ρ hyd	0.0454	g/cc
Sw	Sg	ρb in g/cc	Vp in m/s	Vs in m/s	σ	AI
0.1	0.9	2.09558935	2918.85671	1645.52237	0.26705498	6116.72504
0.2	0.8	2.1215926	2990.866675	1635.40712	0.28674271	6345.40061
0.3	0.7	2.14759585	3080.425548	1625.47616	0.30705192	6615.50912
0.4	0.6	2.1735991	3193.738128	1615.72393	0.32801249	6941.90632
0.5	0.5	2.19960235	3340.516514	1606.14516	0.34965628	7347.80797
0.6	0.4	2.2256056	3536.966232	1596.73476	0.37201725	7871.89185
0.7	0.3	2.25160885	3812.576793	1587.48784	0.39513164	8584.43165
0.8	0.2	2.2776121	4228.152764	1578.39974	0.41903818	9630.0919
0.9	0.1	2.30361535	4936.554275	1569.46596	0.44377831	11371.9222
Calculation for New Gas Zone II						
Input Parameters (Fixed)				Symbol	Value	Unit
Depth				D	1992-2017	m
Temperature				T	51.11	°C
Solid Material Bulk Modulus				Ks	30	Gpa
Solid Material Density				ρs	2.4577	g/cc
Logged P-wave velosity				Vpi	2540	m/s
Logged S-wave velosity				Vsi	1540	m/s
Logged Bulk Density				ρ bi	2.2	g/cc
Fluid Bulk Modulus at logged condition				K fi	1.0878	Gpa
Parameter (Variable)				Symbol	Value	Unit
Pressure				P	19.73279	Mpa
Water Bulk Modulus				Kw	2.523198	GPa
Water Density				ρw	1.0022	g/cc
Hydrocarbon Bulk Modulus				K hyd	0.040273	Gpa
Hydrocarbon Density				ρ hyd	0.1346	g/cc
Sw	Sg	ρb in g/cc	Vp in m/s	Vs in m/s	σ	AI
0.1	0.9	2.1334307	2729.725935	1563.84171	0.25572341	5823.68111
0.2	0.8	2.1460109	2790.885916	1559.25125	0.27310896	5989.2716
0.3	0.7	2.1585911	2863.414022	1554.70097	0.29098267	6180.94002
0.4	0.6	2.1711713	2950.586243	1550.19031	0.30936539	6406.22817
0.5	0.5	2.1837515	3057.12635	1545.71867	0.32827919	6676.00425
0.6	0.4	2.1963317	3190.131988	1541.28551	0.3477474	7006.58801
0.64	0.36	2.20136378	3253.057256	1539.5229	0.35569542	7161.16242
0.7	0.3	2.2089119	3360.838207	1536.89028	0.36779478	7423.79551
0.8	0.2	2.2214921	3588.285493	1532.53243	0.38844756	7971.34788
0.9	0.1	2.2340723	3907.908371	1528.21145	0.40973358	8730.54984
Parameter (Variable)				Symbol	Value	Unit
Pressure				P	17.236893	Mpa
Water Bulk Modulus				Kw	2.506883	GPa
Water Density				ρw	1.0012	g/cc
Hydrocarbon Balk Modulus				K hyd	0.033909	Gpa
Hydrocarbon Density				ρ hyd	0.1182	g/cc
Sw	Sg	ρb in g/cc	Vp in m/s	Vs in m/s	σ	AI
0.1	0.9	2.131276	2632.695017	1564.63202	0.22696096	5610.99971
0.2	0.8	2.1440795	2690.39877	1559.95338	0.24676791	5768.42885
0.3	0.7	2.156883	2759.534441	1555.31646	0.26722484	5951.99292
0.4	0.6	2.1696865	2843.596333	1550.72064	0.28836427	6169.71257
0.5	0.5	2.18249	2947.723805	1546.16533	0.31022094	6433.37773
0.6	0.4	2.1952935	3079.830248	1541.64992	0.33283198	6761.13133

Calculation for New Gas Zone III						
0.7	0.3	2.208097	3252.839175	1537.17385	0.35623714	7182.58442
0.8	0.2	2.2209005	3489.581914	1532.73654	0.38047899	7750.01422
0.9	0.1	2.233704	3835.119202	1528.33743	0.40560321	8566.5211
Parameter (Variable)				Symbol	Value	Unit
Pressure				P	13.789514	Mpa
Water Bulk Modulus				Kw	2.484589	GPa
Water Density				ρw	0.9998	g/cc
Hydrocarbon Balk Modulus				K hyd	0.025843	Gpa
Hydrocarbon Density				ρ hyd	0.0941	g/cc
Sw	Sg	ρb in g/cc	Vp in m/s	Vs in m/s	σ	AI
0.1	0.9	2.12811065	2492.057085	1565.7952	0.17385562	5303.37322
0.2	0.8	2.1412433	2543.324617	1560.98616	0.1978193	5445.8768
0.3	0.7	2.15437595	2605.74497	1556.22116	0.22278176	5613.7543
0.4	0.6	2.1675086	2683.017631	1551.49952	0.24880679	5815.46379
0.5	0.5	2.18064125	2780.743464	1546.82061	0.2759637	6063.8039
0.6	0.4	2.1937739	2907.86359	1542.18377	0.30432798	6379.19525
0.7	0.3	2.20690655	3079.678977	1537.58838	0.33398196	6796.56371
0.8	0.2	2.2200392	3324.999405	1533.03383	0.36501567	7381.62902
0.9	0.1	2.23317185	3706.263383	1528.51952	0.39752769	8276.72305
Parameter (Variable)				Symbol	Value	Unit
Pressure				P	10.342136	Mpa
Water Bulk Modulus				Kw	2.462607	GPa
Water Density				ρw	0.9983	g/cc
Hydrocarbon Balk Modulus				K hyd	0.018437	Gpa
Hydrocarbon Density				ρ hyd	0.0692	g/cc
Sw	Sg	ρb in g/cc	Vp in m/s	Vs in m/s	σ	AI
0.1	0.9	2.12483945	2340.677718	1567.00002	0.09390356	4973.56435
0.2	0.8	2.1383114	2383.083886	1562.05595	0.12334578	5095.77544
0.3	0.7	2.15178335	2435.760627	1557.15839	0.15441668	5241.22916
0.4	0.6	2.1652553	2502.416377	1552.30661	0.18725524	5418.37032
0.5	0.5	2.17872725	2588.847254	1547.4999	0.22201673	5640.39206
0.6	0.4	2.1921992	2704.685366	1542.73756	0.25887514	5929.2091
0.7	0.3	2.20567115	2867.309349	1538.01893	0.29802612	6324.34151
0.8	0.2	2.2191431	3111.956128	1533.34333	0.33969042	6905.87597
0.9	0.1	2.23261505	3524.244468	1528.71011	0.38411808	7868.28124
Parameter (Variable)				Symbol	Value	Unit
Pressure				P	6.894757	Mpa
Water Bulk Modulus				Kw	2.440969	GPa
Water Density				ρw	0.9969	g/cc
Hydrocarbon Balk Modulus				K hyd	0.011539	Gpa
Hydrocarbon Density				ρ hyd	0.0445	g/cc
Sw	Sg	ρb in g/cc	Vp in m/s	Vs in m/s	σ	AI
0.1	0.9	2.1215958	2174.203564	1568.19743	-0.0421808	4612.78115
0.2	0.8	2.1354056	2204.4346	1563.11839	-0.0056176	4707.36199
0.3	0.7	2.1492154	2243.112284	1558.08838	0.03384788	4820.93146
0.4	0.6	2.1630252	2293.580296	1553.10662	0.0765754	4961.07198
0.5	0.5	2.176835	2361.261639	1548.17235	0.12298686	5140.07698
0.6	0.4	2.1906448	2455.603094	1543.2848	0.17358016	5379.35415
0.7	0.3	2.2044546	2594.756297	1538.44325	0.22894717	5720.02245
0.8	0.2	2.2182644	2819.013639	1533.64699	0.28979696	6253.3176
0.9	0.1	2.2320742	3241.896491	1528.89531	0.35698639	7236.15352

Table 9. *The inputs for Shale zones above gas layer and Gas zones for determining AVO.*

Above Shale Zone/Gas Zone	**P-Velocity (Vp)**		**S-Velocity (Vs)**		**Bulk Density (ρ_b) g/cm^3**
	m/sec	**ft/sec**	**m/sec**	**ft/sec**	
Shale Zone Above New gas Zone III	4000	13123	2116	6942	2.40
Shale Zone Above New gas Zone II	3800	12467	2011	6598	2.40
New gas Zone III	2650	8694	1606	5269	2.20
New gas Zone II	2540	8333	1540	5053	2.20

5. Conclusion

The Batzle and Wang model has predicted the fluid properties for both of the constant/varying saturation with constant/varying pressure condition that are near accurate forecasting. Increase of water saturation effects on fluid properties by increasing the fluid density, modulus and acoustic velocity. However, the compressibility of fluid decreases as the water in fluid increases. As temperature increases, the velocity and density of the fluid decrease. The cross plots using the Batzle and Wang model on densities and moduli allows to predict the fluid properties as the reservoir is produced and shows the effect on the reservoir as water saturation increases and gas saturation decreases. The change in P-wave and S- wave velocity, bulk density, acoustic impedance, Poisson's ratio, and bulk modulus were predicted using the Batzle and Wang and Gassmann-Biot model. The result shows that the reservoir changes from irreducible water saturation conditions in residual gas conditions which provide an avenue to calculate values at reservoir conditions from logging conditions. Coupling with the Batzle and Wang (1995), Gassmann-Biot, the AVO models can be used to determine expected seismic responses throughout the production path of the reservoir. In case of the Fenchuganj Gas Field, it is shown that an AVO response is presented as a result of the fluid and rock properties. This modeling results show the reservoir is pressure decreases due to increasing the gas production. The evaluation of fluid properties enables seismic data to be used more effectively. This modeling fluid property will aid in determining the usefulness of time lapse seismic, predicting AVO and amplitude response, and making production and reservoir engineering decisions and forecasting.

Acknowledgment

The authors are grateful to BAPEX authority, especially Geological and Geophysical Division for allowing collecting the necessary data and use their software for this work. The first author is also grateful to Mr. Md. Shofiqul Islam, Geology Division (BAPEX) and Mr. Pulok Kanti Deb, Department of Petroleum and Mining Engineering, Shahjalal University for their help and suggestions to improve this work.

References

[1] Zoeppritz, K., 1919, Erdbebenwellen VIIIB, On the reflection and propagation of seismic waves, Gottinger Nachrichten, I, p. 66-84.

[2] Gassmann, F., 1951, Elastic waves through a packing of spheres: Geophysics, 16, 673-685.

[3] Biot, M. A., 1956, Theory of propagation of elastic waves in a fluid-saturated porous solid: Journal of Acoustical Society of America, 28, 168-191.

[4] Kuster, G.T., and Toksöz, M.N., 1974, Velocity and attenuation of seismic waves in two-phase media: Part I. theoretical formulations: Geophysics, 39, 587-606.

[5] O'Connell R., Budiansky B. 1974, Seismic velocities in dry and saturated crack solids. Journal of geophysical Research, 79, 5412-5426.

[6] Rutherford, S.R. and Williams, R.H., 1989, Amplitude-versus-offset variations in gas sands: Geophysics, 54, 680-688.

[7] Mavko, G., and Jizba, D. 1991, Estimating grain-scale fluid effects on velocity dispersion in rocks, Geophysics, 56(12), 1940–1949, doi:10.1190/1.1443005.

[8] Batzle, M. and Wang, Z., 1992, Seismic properties of pore fluids: Geophysics, Vol. 57(11), 1396-1408.

[9] Sheriff, R.E., 1991, Encyclopedic Dictionary of Exploration Geophysics, 3rd Edition: SEG Geophysical References Series 1, Tulsa, USA, p. 384.

[10] Castagna, J.P. and Swan, H.W., 1997, Principles of AVO crossplotting: The Leading Edge, 16, 337-342.

[11] Bulloch, T.E., 1999, The Investigation Of Fluid Properties And Seismic Attributes For Reservoir Characterization, M.Sc thesis for Geological Engineering, Michigan TechnologicaI University, USA.

[12] Annual Report, 2010, Bangladesh Petroleum Exploration and Production Company Limited (BAPEX), Bangladesh

[13] Mannan, M. A., 2002, Stratigraphic evolution and geochemistry of the Neogene Surma Group, Surma Basin, Sylhet, Bangladesh, PhD Dissertation, Department of Geology, University of Oulu.

[14] Farhaduzzaman, M., Wan Hasiah A., Islam, M. A., and Pearson, M. J., 2012, Source rock potential of the organic-rich shales in the Tertiary Bhuban and BokaBil Formations, Bengal Basin, Bangladesh. Journal of Petroleum Geology, 35 (4), 357-376.

[15] Sheriff, R.E., and Geldart, L.P., 1995, Exploration Seismology, 2nd Edition: Cambridge University Press, New York, USA, p. 592.

[16] Murphy, W.F., Schwartz, L.M., and Hornby, B., 1991, Interpretation physics of Vp and Vs in sedimentary rocks: Transactions SPWLA 32nd Annual Logging Symp., p. 1-24.

[17] Schlumberger Oilfield Glossary. (URL: http://www.glossary.oilfield.slb.com/en/Terms.aspx?LookIn=term%20name&filter=amplitude%20variation%20with%20offset)

[18] Mavko, G., Mukerji, T., Dvorkin, J., 1998, The Rock Physics Handbook: Tools for Seismic Analysis in Porous Media: Cambridge University Press, Cambridge, New York, USA, 329 pp.

[19] Castagna, J. P., and Backus, M. M., 1993, Offset-Dependent Reflectivity -Theory and Practice of AVO Analysis: SEG Investigations in Geophysics Series, 8, Tulsa, USA, 348.

[20] Hales, A.L., and Roberts, J.L., 1974, The Zoeppritz amplitude equations: more errors: Bulletin of Seismological Society of America, Vol. 64, p. 285.

[21] Aki, K., and Richards, P.G., 1980, Quantitative seismology: Theory and methods: W. H. Freeman and Co.

[22] Shuey, R.T., 1985, A simplification of the Zoeppritz equations: Geophysics, 50, 609-614

[23] Hilterman, F., 1989, Is AVO the seismic signature of rock properties? 59th Ann. Internat. Mtg., Soc. Expl. Geophys., Expanded Abstracts, 559.

[24] Knigh R, Nolen-Hoeksema R. A., 1990, laboratory study of the dependence of elastic wave velocities on pore scale fluid distribution. Geophysical Research Letters, 17 (10), 1529-1532.

[25] Liu Zhupin, WU Xiaowei, Chu Zehan 1994, Laboratory study of acoustic parameters of rock. Chinese Journal of Geophysics (Acta Geophysica Sinica), 37 (5): 659-666.

[26] Gregory A R. Fluid saturation on dynamic elastic properties of sedimentary rocks. Geophysics, 1976, 41 (5), 895-921.

[27] Lee, M.W., 2003, Elastic Properties of Overpressured and Unconsolidated Sediments, U.S. Geological Survey Bulletin 2214, Version 1.0, 1-10.

[28] Gardner, G. H. F. and Harris, M.H., 1968, Velocity and attenuation of elastic waves in sands: Society of Professional Well Log Analysts, Transactions, 9th Annual Log Symposium, p. M1–M19.

[29] Pickett, G.R., 1963, Acoustic character logs and their applications in formation evaluation: Journal of Petroleum Technology, 15, 650–667.

[30] Deb, P. K., 2011, An application of seismic and well log techniques to the structural and stratigraphic development of Fenchuganj Gas Field, B.Sc thesis, Department of Petroleum and Mining Engineering, SUST, Bangladesh.